Structural, Elastic, Electronic, and Optical Properties of Cubic Perovskite $CsCaCl_3$ Compound: An *ab initio* Study

K. Ephraim Babu, N. Murali, K. Vijaya Babu, Paulos Taddesse Shibeshi and V. Veeraiah*

Modelling and Simulation in Materials Science Laboratory, Department of Physics, Andhra University Visakhapatnam, Andhra Pradesh, 530003, India

(Received May 2, 2013; in final form December 12, 2013)

Structural, elastic, electronic, and optical properties of cubic perovskite $CsCaCl_3$ are calculated using the full-potential linearized augmented plane wave method in the density functional theory. The exchange-correlation potential is evaluated using the local density approximation and generalized gradient approximation. Further, the modified Becke–Johnson potential is also applied for studying the electronic and optical properties. The calculated structural properties such as equilibrium lattice constant, the bulk modulus and its pressure derivative are in good agreement with the available data. The elastic properties such as elastic constants, anisotropy factor, shear modulus, Young's modulus and Poisson's ratio are calculated. The calculations of electronic band structure, density of states and charge density show that this compound has an indirect energy band gap (M–Γ) with a mixed ionic and covalent bonding. Calculations of the optical spectra such as the real and imaginary parts of dielectric function, optical reflectivity, absorption coefficient, optical conductivity, refractive index, extinction coefficient and electron energy loss are performed for the energy range of 0–30 eV. Most of the studied properties are reported for the first time for $CsCaCl_3$.

DOI: 10.12693/APhysPolA.125.1179

PACS: 71.15.Mb, 71.15.Ap, 71.20.–b

1. Introduction

The scintillation detector is one of the most widely used radiation detectors. At present there is a strong interest in development of new fast inorganic scintillates for applications in high-energy physics, medical diagnostics and materials science. Scintillator crystals provide effective radiation sensors that can be used in advanced medical imaging, enhanced security from nuclear threats and many other related applications. The ultimate performance of a single crystal scintillator-based radiation monitoring device is strongly tied to both the physical and the scintillation properties of the crystals. The ternary chlorides having the perovskite structure show many potential applications due to their wide band gaps and optical properties [1, 2]. The crystals of ABX_3 (A is a cation with different valence, B is a transition metal, and X is oxide or halide) type which crystallize in a perovskite-like structure are acousto-optic materials of interest [3]. These crystals are also model substances for the study of phase transition. For example, the $CsCaCl_3$ is a cubic chloride perovskite at room temperature ($Pm\text{-}3m$). It undergoes a cubic to tetragonal phase transition at low temperature ($T_c = 95$ K) [4, 5]. $CsCaCl_3$ melts congruently at 1182 K and crystallizes in a cubic structure [6]. Crystalline $CsCaCl_3$ has been previously reported as a self-activated scintillator with core–valence luminescence [7]. Features of the core–valence luminescence and electron energy band structure of $CsCaCl_3$ are also reported [8]. Photoluminescence, thermal luminescence, and luminescence excitation spectra of $CsCaCl_3$ (pure and impure) in the temperature range 79–350 K [9] have been investigated and reported. Hence, $CsCaCl_3$ is a potential compound for crystal scintillators [10, 11].

Our aim in this paper is to investigate the structural, elastic, electronic, and optical properties of $CsCaCl_3$ compound using a recent technique called "modified Becke–Johnson potential" (mBJ). The mBJ is known for overcoming the problem of underestimation of bandgap in case of local density approximation (LDA) and generalized gradient approximation (GGA). To the best of the authors' knowledge, density of states (DOS) has been reported by Chornodolskyy et al. [8], electronic structure and optical properties have been reported by Tyagi et al. [12], using GGA approximation. Moreover, neither experimental nor theoretical efforts have been made by them to discern the elastic properties like elastic constants, anisotropy factor, shear modulus, Young's modulus, Poisson's ratio for this compound.

In this work, we will contribute to the study of the perovskite chloride $CsCaCl_3$ by performing a first-principles investigation of their structural, elastic, electronic, and optical properties using the full potential linearized augmented plane wave (FP-LAPW) method in the density functional theory (DFT) framework within GGA and LDA using the WIEN2K code [13]. The use of first-principles calculations offers one of the most powerful tools for carrying out theoretical studies of an important number of physical and chemical properties of the condensed matter with great accuracy [14, 15].

The paper is organized as follows. After a brief introduction in Sect. 1, the theoretical framework within which all the calculations have been performed is out-

*corresponding author; e-mail: v_veeraiah@yahoo.co.in

lined in Sect. 2. We present and discuss the results of our study in Sect. 3. A conclusion of the present investigation is given in Sect. 4.

2. Computational details

The first-principles calculations are performed using the full potential linearized augmented plane wave (FP--LAPW) method as implemented in WIEN2K code [13]. The exchange-correlation potential is calculated within the local density approximation (LDA) [16] or generalized gradient approximation (GGA) by Perdew–Burke–Ernzerhof (PBE) [17] or Wu and Cohen (WC–GGA) [18]. The recent mBJ [19] is also applied to calculate the electronic and optical properties of this compound. In this FP-LAPW method, there are no shape approximations to the charge density or potential. Space is divided into two regions, a spherical muffin-tin (MT) around the nuclei in which the radial solutions of the Schrödinger equation and their energy derivatives are used as basis functions, and the interstitial region between the muffin-tins, in which the basis set consists of plane waves. The cut--off energy which defines the separation between the core and valence states is set at -6.0 Ry. The sphere radii used are 2.0 a.u. for Cs, 1.8 a.u. for Ca and 1.5 a.u. for Cl, respectively. The experimental lattice constant is $a_0 = 5.396$ Å as reported by Moreira and Dias [20] and other works [5, 8]. Augmented plane wave (APW) plus local valence orbitals are used with the wave functions, while the potentials and charge densities are expanded in terms of spherical harmonics inside the muffin--tin spheres. The Brillouin zone integration is carried out by using the modified tetrahedron method [21] up to 35 k-points in the irreducible wedge of the simple cubic Brillouin zone. Well-converged solutions were obtained with $R_{\mathrm{MT}}\, K_{\max} = 7.0$ (where R_{MT} is the smallest of the muffin-tin radii and $K_{\max}$ is the plane wave cut-off) and k-point sampling is checked. Self-consistent calculations are considered to be converged when the total energy of the system is stable within 0.0001 Ry. The optoelectronic properties of the compound are calculated using a denser mesh of 364 k-points in the irreducible Brillouin zone (IBZ).

3. Results and discussion

3.1. Structural properties

The perovskite $CsCaCl_3$ compound has ideal cubic structure with space group *Pm-3m* (#221). The atomic positions in the elementary cell are at Cs (0, 0, 0), Ca (0.5, 0.5, 0.5) and Cl (0, 0.5, 0.5). Figure 1 shows the crystal structure of $CsCaCl_3$. The volume versus energy is fitted by the Birch–Murnaghan equation of state [22]. From this fit, we can get the equilibrium lattice constant (a_0), bulk modulus (B_0) and pressure derivative of the bulk modulus (B'). These values are shown in Table I.

We performed our calculations by using LDA and GGA approximations. The total energy per unit cell of $CsCaCl_3$ in the cubic perovskite structure is shown in Fig. 2. Our calculated equilibrium lattice parameter (a_0) is in reasonable agreement with the experimental

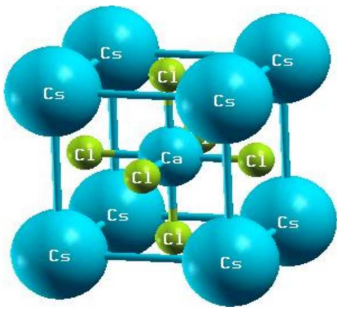

Fig. 1. Crystal structure of $CsCaCl_3$ obtained with XCrysDen.

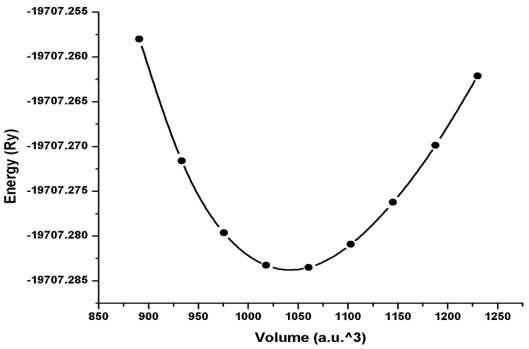

Fig. 2. Dependence of total energy of cubic perovskite $CsCaCl_3$ crystal on unit cell volume (using GGA–WC).

value. The bulk modulus (B_0) is a measure of the crystal rigidity, thus a large value of B_0 indicates high crystal rigidity. No previous experimental or theoretical result for this parameter is available for the $CsCaCl_3$ compound for comparison with the present calculation.

3.2. Elastic properties

The elastic constants C_{ij} are fundamental and indispensable for describing the mechanical properties of materials. The elastic constants are important parameters that describe the response to an applied macroscopic stress. The elastic constants of solids provide a link between the mechanical and dynamical behaviour of crystals, and define how a material undergoes stress deformations and then recovers and return to its original shape af-

TABLE I

Calculated lattice constant a_0 [Å], bulk modulus B_0 [GPa] and pressure derivative (B'), ground state energy (E_0) of $CsCaCl_3$.

Method	Lattice constant a_0 [Å]	B_0 [GPa]	B'	E_0 [Ry]
LDA	5.248	32.897	4.727	−19687.992
GGA–WC	5.369	25.692	4.804	−19707.283
GGA–PBE	5.474	23.640	4.513	−19711.220
Expt.	5.396[a]			

[a] Ref. [20], experimental value.

ter stress ceases [23]. The elastic constants are important parameters of a material and can provide valuable information about the structural stability, the bonding character between adjacent atomic planes, and anisotropic character. For cubic system, there are three independent elastic constants C_{11}, C_{12} and C_{44}. In order to determine them, the cubic unit cell is deformed using an appropriate strain tensor to yield an energy-strain relation. In this work, we have used the method developed by Charpin and implemented in the WIEN2K package [13].

TABLE II

Calculated elastic constants and the bulk modulus (B), anisotropy factor A, shear modulus G (in GPa), Young's modulus E (in GPa) and Poisson's ratio υ of $CsCaCl_3$.

	C_{11}	C_{12}	C_{44}	B	A	G	E	υ	B/G
LDA	76.879	10.990	11.525	32.953	0.349	17.834	45.325	0.270	1.847
GGA	56.905	9.692	10.233	25.430	0.433	14.406	36.353	0.363	1.765

In Table II we summarize the calculated elastic constants and the bulk modulus. From Table II, we remark that the calculated elastic constants within the LDA are higher than the GGA calculated values. The obtained bulk modulus using the LDA is higher than that obtained within the GGA. The calculated elastic constants C_{ij} are positive and satisfy the mechanical stability criteria [24] in a cubic crystal: $(C_{11} - C_{12}) > 0$; $(C_{11} + 2C_{12}) > 0$; $C_{11} > 0$; $C_{44} > 0$, and the bulk modulus B also should satisfy a criterion: $C_{12} < B < C_{11}$.

The bulk modulus calculated from the elastic constants $B = (1/3)(C_{11} + 2C_{12})$ within the LDA and GGA approximations is in good agreement with that obtained from the total energy minimization calculations (see Table I). One can notice that the unidirectional elastic constant C_{11}, which is related to the unidirectional compression along the principal crystallographic directions, is about 85.01% for LDA and 82.01% for GGA, indicating that this compound presents a weaker resistance to the unidirectional compression. To the best of our knowledge no experimental or theoretical values for the elastic constants of this material have been published; hence our results can serve as a reference for future investigations. Similar work to calculate elastic properties has been reported in the literature [25–27]. The anisotropy factor (A), Young's modulus (E), Shear modulus (G) and Poisson's ratio υ which are the most interesting elastic constants (are listed in Table II), by using the following relations [28]:

$$A = \frac{2C_{44}}{C_{11} - C_{12}}, \tag{1}$$

$$E = \frac{9GB}{3B + G}, \tag{2}$$

$$\nu = \frac{3B - 2G}{2(2B + G)}, \tag{3}$$

$$G = \frac{1}{2}(G_{\mathrm{V}} + G_{\mathrm{R}}), \tag{4}$$

$$G_{\mathrm{V}} = \frac{1}{5}(C_{11} - C_{12} + 3C_{44}), \tag{5}$$

$$G_{\mathrm{R}} = \frac{5C_{44}(C_{11} - C_{12})}{4C_{44} + 3(C_{11} - C_{12})}, \tag{6}$$

where G is the shear modulus, G_{V} is Voigt's shear modulus corresponding to the upper bound of G values and G_{R} is Reuss's shear modulus corresponding to the lower bound of G values. The anisotropy factor (A) is equal to one for an isotropic material, while any value smaller or larger than one indicates anisotropy. The magnitude of the deviation from 1 is a measure of the degree of elastic anisotropy possessed by the crystal. We obtain that the value of the anisotropy factor A is 0.349 in the LDA (0.433 in the GGA). This indicates that our compound is anisotropic.

Young's modulus (E) is a good indicator about the stiffness of the material. When it is higher for a given material, the material is stiffer. Poisson's ratio provides more information for dealing with the characteristic of the bonding forces than does any of the other elastic property. The value of the Poisson ratio (υ) for covalent materials is small ($\upsilon < 0.1$), whereas for ionic materials a typical value of υ is 0.25 [29]. In our calculations υ is 0.270 for LDA and 0.363 for GGA. Hence, a higher ionic contribution in an intra-atomic bonding for this compound should be assumed. Mechanical properties such as ductility and brittleness of materials can be explained from the proposed relationship. The shear modulus G represents the resistance to plastic deformation, while the bulk modulus B represents the resistance to fracture. We know that there is a criterion for B/G ratio which separates the ductility and brittleness of materials. According to Pugh's criteria [30], the critical value is 1.75 i.e., if $B/G > 1.75$ the material is ductile, otherwise it is brittle. For the $CsCaCl_3$, the B/G ratio is 1.847 within LDA and 1.765 within the GGA, thus according to Pugh's criteria, our material is ductile.

3.3. Band structure and density of states

Now we discuss our results of the electronic properties of $CsCaCl_3$ via the energy band, the total and partial density of states. We have applied the LDA, GGA and mBJ methods to calculate these properties. The calculated band structure for $CsCaCl_3$ using LDA, GGA–PBE, GGA–WC and mBJ along high symmetry directions in the first Brillouin zone at equilibrium volume are given in Fig. 3. The calculated values of the band gaps are found to be equal to 5.29, 5.35, 5.43, and 6.93 eV using LDA, GGA–PBE, GGA–WC, and mBJ, respectively. The calculated LDA and GGA band gap values for $CsCaCl_3$ are in excellent agreement with those obtained by Chornodolskyy et al. [8] and Tyagi et al. [12]. As the DFT within both LDA and GGA is known to underestimate the band gap values, the latest approach of mBJ is used to remove this discrepancy and to obtain a reliable band gap for the $CsCaCl_3$ compound.

The results obtained in the present work are very close to the experimental/predicted values of other researchers than the results presented in the paper by Tyagi et al. Hence we conclude that mBJ method is more suitable for the study of $CsCaCl_3$ compound. The mBJ–GGA potential V_{xc} uses the mBJ exchange potential plus the GGA correlation potential and performs the calculations of band gap precisely. This method provides the band gaps almost equal to the experimental values [19]. The calculated energy bands along the high symmetry lines in the Brillouin zone and total as well as partial density of states of $CsCaCl_3$ are shown in Figs. 3 and 4, respectively. The zero of energy is chosen to coincide with the valence band maximum (VBM), which occurs at M point, and the conduction band minimum (CBM) occurs at the Γ point resulting in an indirect band gap of 6.943 eV.

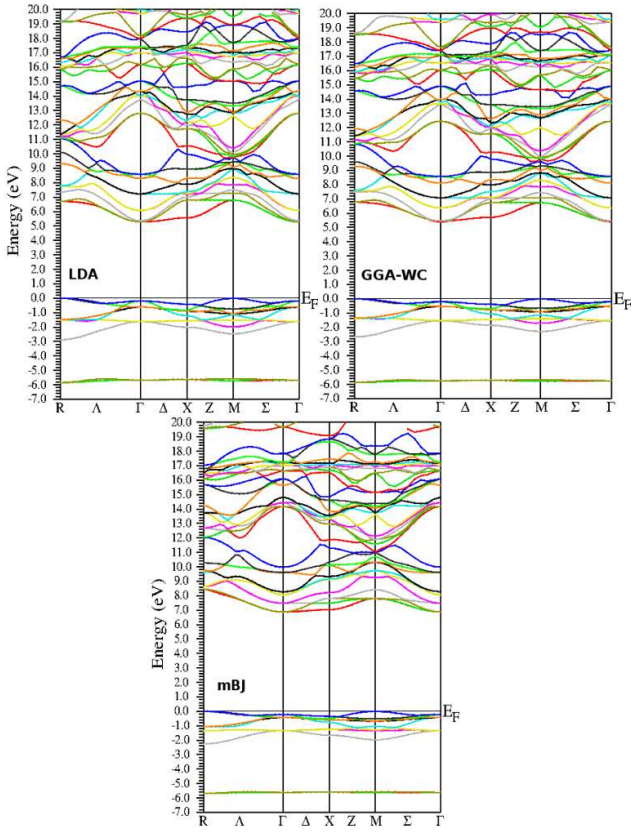

Fig. 3. Band structure of $CsCaCl_3$ along the high symmetry point.

On the basis of different bands; the total density of states (TDOS) could be grouped into four regions and the contribution of different states in these bands can be seen from the partial density of states (PDOS). The first region around −6.0 eV comprising a narrow band due to the Cs 5p state is clearly seen from Fig. 4b. In the second region around −2.8 eV to the Fermi energy level, majority contribution is due to Cl 3p states (seen in Fig. 4d) and minority contribution is due to Ca 3d states. There is hybridization between Ca 3d with Cl 3p states in this

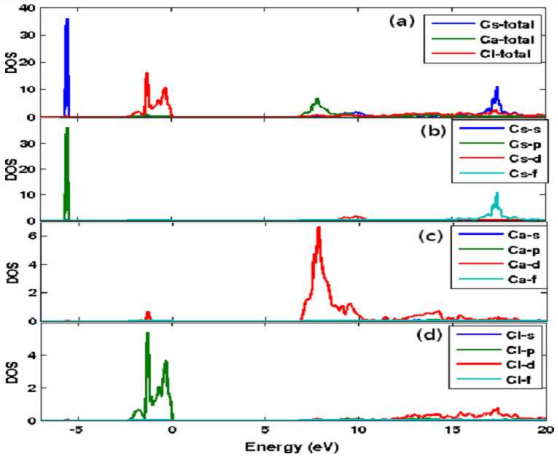

Fig. 4. (a) Total and partial density of states, (b) Cs, (c) Ca, and (d) Cl in $CsCaCl_3$.

region. The first and second regions within the range of −6.0 to 0 eV comprise the valence band. The upper part of the valence band is composed of the Cl 3p and Ca 3d states. The third region above the Fermi level is the conduction band. The lower part of this band near the Fermi level is mainly due to the contributions from Cl 3p, Cl 3s, and Ca 3p states. In the conduction band from 7.0 eV to 10 eV majority contribution is from Ca 3d states. Along with this majority contribution from Ca 3d states, there are minor contributions from Cs 5d and Cl 2p states observed. From 10 to 20 eV a small contribution is due to the Cs 4f, Cl 3d, Ca 3d, and Cs 5d states in the conduction band. The band gap has been measured experimentally for $CsCaCl_3$ by Macdonald et al. [31]. Our theoretical calculations are in good agreement with their results. The calculated band gap of $CsCaCl_3$ is shown in Table III.

TABLE III

Energy gap at high symmetry points for $CsCaCl_3$.

	M–Γ	Γ–Γ	R–X	R–M	M–M	R–R	R–Γ	X–X
LDA	5.29	5.44	5.59	6.77	6.77	6.74	5.29	5.98
GGA–PBE	5.35	5.50	5.80	6.65	6.65	6.86	5.35	6.13
GGA–WC	5.43	5.61	5.73	6.74	6.74	6.77	5.43	6.05
mBJ–GGA	6.93	7.08	7.10	7.85	7.85	8.48	6.93	7.40

The charge density distributions are shown in Fig. 5. Charge density maps serve as a complementary tool for achieving a proper understanding of the electronic structure of the system being studied. The ionic character of any material can be related to the charge transfer between the cation and anion while covalent character is related to the sharing of the charge among the cation and anion. The covalent behaviour is due to hybridization of Ca d and Cs p with the Cl p states in the valence band near the Fermi energy level.

From the figures it is clear that the highest charge density occurs in the immediate vicinity of the nuclei. The

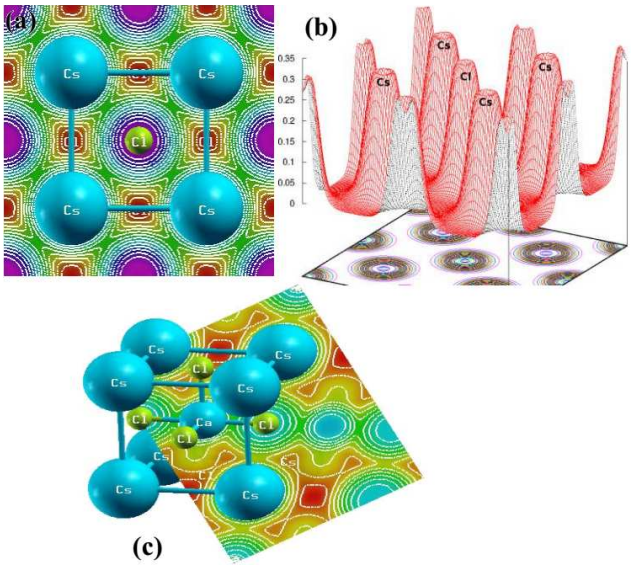

Fig. 5. Charge density distribution of $CsCaCl_3$ (a) along (1 0 0) plane in 2D representation, (b) along (1 0 0) plane in 3D representation, (c) along (1 1 0) direction.

near spherical charge distribution around Cs indicates that the bond between Cs and Cl is strong ionic, with no charge sharing among the contours of the respective atoms. It can be seen that most of the charge is populated in the Ca–Cl bond direction, while the maximum charge resides on the Ca and Cl sites. The corresponding contour maps of the charge density distributions are shown in Fig. 5a along (1 0 0) plane in 2D representation, Fig. 5b along (1 0 0) plane in 3D representation and Fig. 5c along (1 1 0) plane in 2D representation. Hence, we conclude that there exists a strong ionic bonding in Cs–Cl and a mixture of ionic and weak covalent bonding in Ca–Cl_2. Similar bonding nature has been predicted for other compounds like to $CsCaCl_3$, e.g., $CsCaF_3$ [32] and $CsSrF_3$ [33].

3.4. Dielectric and optical properties

The dielectric function $\varepsilon(\omega) = \varepsilon_1(\omega) + \mathrm{i}\varepsilon_2(\omega)$ is known to describe the optical response of the medium at all photon energies. The imaginary part $\varepsilon_2(\omega)$ is directly related to the electronic band structure of a material and describes the absorptive behaviour. The imaginary part of the dielectric function $\varepsilon_2(\omega)$ is given [34, 35] by

$$\varepsilon_2(\omega) = \left(\frac{4\pi^2 e^2}{m^2\omega^2}\right) \sum_{i,j} \int_k \langle i|M|j\rangle^2 f_i(1-f_i) \times \delta(E_{j,k} - E_{i,k} - \omega)\,\mathrm{d}^3k, \quad (7)$$

where M is the dipole matrix, i and j are the initial and final states, respectively, f_i is the Fermi distribution function for the i-th state, and E_i is the energy of electron in the i-th state with crystal wave vector k. The real part $\varepsilon_1(\omega)$ of the dielectric function can be extracted from the imaginary part using the Kramers–Kronig relation in the form [36, 37]:

$$\varepsilon_1(\omega) = 1 + \frac{2}{\pi}\mathrm{P}\int_0^\infty \frac{\omega'\varepsilon_2(\omega')\,\mathrm{d}\omega'}{\omega'^2 - \omega^2}, \quad (8)$$

where P implies the principal value of the integral.

The FP-LAPW is a good theoretical tool for the calculation of the optical properties of a compound. The optical properties give useful information about the internal structure of the $CsCaCl_3$ compound. The mBJ–GGA method is used to calculate the optical properties of this compound.

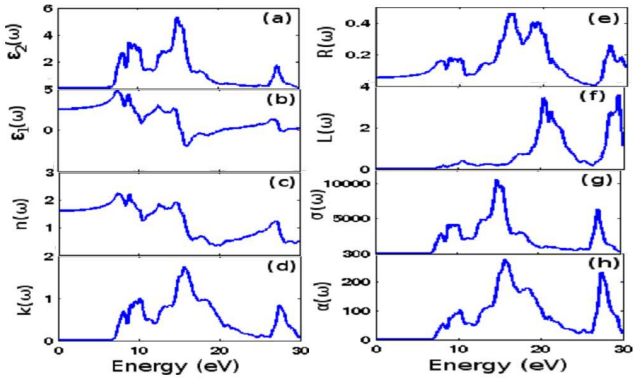

Fig. 6. Optical spectra as a function of photon energy for cubic perovskite $CsCaCl_3$. (a) Imaginary part $\varepsilon_2(\omega)$ and (b) real part $\varepsilon_1(\omega)$ of dielectric function, (c) refractive index $n(\omega)$, (d) extinction coefficient $k(\omega)$, (e) reflectivity $R(\omega)$, (f) energy loss function $L(\omega)$, (g) optical conductivity $\sigma(\omega)$, and (h) absorption coefficient $\alpha(\omega)$ of $CsCaCl_3$.

The calculated optical properties of $CsCaCl_3$ are shown in Fig. 6. The imaginary part $\varepsilon_2(\omega)$ and the real part $\varepsilon_1(\omega)$ of the dielectric function, refractive index $n(\omega)$, extinction coefficient $k(\omega)$, reflectivity $R(\omega)$, energy loss function $L(\omega)$, optical conductivity $\sigma(\omega)$ and absorption coefficient $\alpha(\omega)$ of $CsCaCl_3$ are shown in Fig. 6, as functions of the photon energy in the range of 0–30 eV. The imaginary part $\varepsilon_2(\omega)$ gives the information of absorption behaviour of $CsCaCl_3$. In the imaginary part $\varepsilon_2(\omega)$, the threshold energy of the dielectric function occurs at $E_0 = 6.93$ eV, which corresponds to the fundamental gap at equilibrium. It is well known that the materials with band gaps larger than 3.1 eV work well for applications in the ultraviolet (UV) region of the spectrum [38, 39]. Hence this wide band gap material could be suitable for the high frequency UV device applications.

>From Fig. 6a for the imaginary part $\varepsilon_2(\omega)$, it is clear that there is a strong absorption peak in the energy range of 7.09–20.0 eV. So, it can also be used as a filter for various energies in the UV spectrum. The maximum absorption peak is at 14.92 eV. The peaks around 8.0 eV to 10.23 eV appear due to the electronic transition from Cs $5p$ state of the valence band (VB) to the unoccupied Ca $3d$ and Cs $5d$ states in the conduction band (CB). The peaks in the range of 12.63–20 eV appear due to the transitions from Cs $5p$ state of the VB to the unoccupied Cs $4f$, and Cl $3d$ states of the CB.

The real part of the dielectric function $\varepsilon_1(\omega)$ is displayed in Fig. 6b. This function $\varepsilon_1(\omega)$ gives us information about the electronic polarizability of a material. The static dielectric constant at zero is obtained as $\varepsilon_1(0) = 2.56$. From its zero frequency limit, it starts increasing and reaches the maximum value of 4.89 at 7.40 eV, and goes below 0 in negative scale for the ranges of 15.24–20.46 eV and 27.44–28.29 eV.

The refractive index and extinction coefficient are displayed in Fig. 6c and d. In Fig. 6c, we observe the optically isotropic nature of this compound in the lower energy range. For lower energies the refractive index value is almost constant and as the energy increases it attains a maximum value and exhibits decreasing tendency for higher energy values. The static refractive index $n(0)$ is found to have the value 1.60. It increases with energy in the transparent region reaching a peak in the ultraviolet range at 7.40 eV. The refractive index is greater than one because as photons enter a material they are slowed down by the interaction with electrons. The more photons are slowed down while travelling through a material, the greater the material's refractive index. Generally, any mechanism that increases electron density in a material also increases refractive index.

However, refractive index is also closely related to bonding. In general, ionic compounds are having lower values of refractive index than covalent ones. In covalent bonding more electrons are being shared by the ions than in ionic bonding and hence more electrons are distributed through the structure and interact with the incident photons to slow down. The refractive index of the compound starts decreasing beyond maximum value and goes below one for the range given in Table IV. Refractive index less than unity ($V_g = c/n$) shows that the group velocity of the incident radiation is greater than c.

TABLE IV

Calculated zero frequency limits of refractive index $n(0)$, reflectivity $R(0)$, energy range for $n(\omega) < 1$, maximum values of refractive index $n(\omega)$, reflectivity $R(\omega)$, and optical conductivity $\sigma(\omega)$ of $CsCaCl_3$.

$CsCaCl_3$	$n(0)$	Maxi-mum $n(\omega)$	Energy range (in eV) for $n(\omega) < 1$	$R(0)$ [%]	Maxi-mum $R(\omega)$	Maximum $\sigma(\omega)$ (in Ω^{-1} cm^{-1})
this work	1.60	2.217	15.85–26.21 27.37–30.00	5.34	46.03	10618.90

When we look at the behaviour of imaginary part of dielectric function $\varepsilon_2(\omega)$ and extinction coefficient $k(\omega)$, a similar trend is observed from Fig. 6a and d. The extinction coefficient $k(\omega)$ reaches the maximum absorption in the medium at 15.74 eV. Frequency dependent refractive index $n(\omega)$, reflectivity $R(\omega)$, and optical conductivity $\sigma(\omega)$ are also calculated and the salient features of the spectra are presented in Table IV.

The optical reflectivity $R(\omega)$ is displayed in Fig. 6e and the zero-frequency reflectivity is 5.34%, which remains almost the same up to 5.10 eV. The maximum reflectivity value is about 46.03% which occurs at 16.14 eV. Interestingly, the maximum reflectivity occurs where the real part of dielectric function $\varepsilon_1(\omega)$ goes below zero, as seen from Fig. 6b and e.

The energy loss function $L(\omega)$ is displayed in Fig. 6f. This function $L(\omega)$ is an important factor describing the energy loss of a fast electron traversing in a material. The peaks in $L(\omega)$ spectra represent the characteristic associated with the plasma resonance. The resonant energy loss is seen at 20.40 eV.

The optical conductivity $\sigma(\omega)$ is shown in Fig. 6g. It starts from 6.95 eV and the maximum value of optical conductivity of the compound is obtained at 14.91 eV with a magnitude of 10618.9 Ω^{-1} cm^{-1}.

Similar features are also observed in absorption coefficient $\alpha(\omega)$ in the absorption range up to 30 eV and it is shown in Fig. 6h. Absorption spectra and electronic structure provide basic understanding of scintillating characteristics of materials. The imaginary part $\varepsilon_2(\omega)$ of the dielectric function is directly proportional to the absorption spectra. The maximum absorption occurs at 15.74 eV. $CsCaCl_3$ is a wide band gap compound with high absorption power in ultraviolet energy range and hence it can be used in the optoelectronic devices like UV detectors. This compound is found to be optically isotropic in the lower energy region, though it is structurally anisotropic, which is the main requirement for the scintillator applications. This type of work is reported in the literature [40]. The above mentioned optical parameters strongly depend on the band structure and our results are in agreement with the results of Tyagi et al. [12] and Macdonald et al. [31].

In order to consider the number of valence electrons per unit cell involved in the interband transitions we evaluate the sum rule. The effective number of the electrons, n_{eff} taking part in transition up to frequency ω can be calculated by using the following sum rule [37]:

$$n_{\text{eff}}(\omega) = \int_0^{\omega} \sigma(\dot{\omega})\dot{\omega}. \tag{9}$$

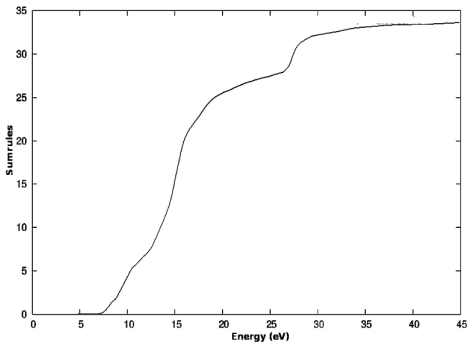

Fig. 7. Frequency dependent sum rules for $CsCaCl_3$.

In Fig. 7 the oscillator strength sum rule for $CsCaCl_3$ is shown. It is clear from the figure up to 6.93 eV the effective number of electrons is zero for this compound. Then it rises gradually at low energies while a rapid change can be seen at above 16 eV. The effective number of elec-

trons saturates at about 38.60 eV with a value of 33.35. The highest contribution to this comes from the Cs $5p$ orbitals as compared to others.

4. Conclusions

In this work, we have studied the structural, elastic, electronic, and optical properties of the cubic perovskite $CsCaCl_3$ using the FP-LAPW method within the local density approximation (LDA), generalized gradient approximation (GGA) in the framework of density functional theory. The estimated lattice constant is found to be in good agreement with the experimental result. We have predicted some elastic properties such as elastic constants, anisotropy factor, shear modulus, Young's modulus and the Poisson ratio. Much improved electronic and optical properties of $CsCaCl_3$ have been calculated by using a new technique known as mBJ potential. The compound exhibits strong ionic bonding in Cs–Cl and a mixture of ionic and weak covalent bonding in Ca–Cl_2. The optical properties such as dielectric function, reflectivity, absorption coefficient, real part of optical conductivity, refractive index, extinction coefficient, and electron energy loss are studied in the energy range of 0–30 eV. Our calculations reveal that $CsCaCl_3$ is a wide band gap material with optically isotropic and structurally anisotropic property, which indicate that it is a better candidate for scintillator applications.

References

[1] R. Hua, B. Lei, D. Xie, C. Shi, *J. Solid State Chem.* **175**, 284 (2003).

[2] K. Shimamura, H. Sato, A. Bensalah, V. Sudesh, H. Machida, N. Sarukura, T. Fukuda, *Cryst. Res. Technol.* **36**, 801 (2001).

[3] S.V. Melnikova, A.T. Anistratov, B.V. Beznosikov, *Sov. Phys. Solid State* **19**, 1266 (1977).

[4] Y. Vaills, J.Y. Buzare, A. Gibaud, Ch. Launay, *Solid State Commun.* **60**, 139 (1986).

[5] H.E. Swanson, H.F. McMurdie, M.C. Morris, E.H. Evans, Nat. Bur. Stand. (U.S.), Monogr. 25, Section 5, 1967, p. 94.

[6] G.S. Perry, K.N. Moody, *Thermochim. Acta* **198**, 167 (1992).

[7] P.A. Rodnyi, I.H. Munro, M.A. Macdonald, E.N. Melchakov, S.S. Kotelnikov, A.S. Voloshinovsky, *Nucl. Instrum. Methods Phys. Res.* **88**, 407 (1994).

[8] Ya. Chornodolskyy, G. Stryganyuk, S. Syrotyuk, A. Voloshinovskii, P. Rodnyi, *J. Phys., Condens. Matter* **19**, 476211 (2007).

[9] I.P. Pashuk, N.S. Pidzyrailo, Z.A. Khapko, *Russ. Phys. J.* **20**, 1081 (1977).

[10] C.W.E. Van Eijk, *Nucl. Tracks Radiat. Meas.* **21**, 5 (1993).

[11] M. Zhuravleva, B. Blalock, K. Yang, M. Koschan, C.L. Melcher, *J. Cryst. Growth* **352**, 115 (2012).

[12] Mohit Tyagi, M. Zhuravleva, C.L. Melcher, *J. Appl. Phys.* **113**, 203504 (2013).

[13] P. Blaha, K. Schwarz, G.K.H. Madsen, D. Kvasnicka, J. Luitz, in: *WIEN2K: An Augmented Plane Wave Plus Local Orbitals Program for Calculating Crystal Properties*, Ed. K. Schwarz, Vienna Technological University, Vienna, Austria 2001.

[14] P. Goudochnikov, A.J. Bell, *J. Phys. Condens. Matter* **19**, 176201 (2007).

[15] C.M.I. Okoye, *Mater. Sci. Eng. B* **130**, 101 (2006).

[16] J.P. Perdew, Y. Wang, *Phys. Rev. B* **45**, 13244 (1992).

[17] J.P. Perdew, K. Burke, M. Ernzerhof, *Phys. Rev. Lett.* **77**, 3865 (1996).

[18] Z. Wu, R.E. Cohen, *Phys. Rev. B* **73**, 235116 (2006).

[19] F. Tran, P. Blaha, *Phys. Rev. Lett.* **102**, 226401 (2009).

[20] R.L. Moreira, A. Dias, *J. Phys. Chem. Solids* **68**, 1617 (2007).

[21] P.E. Blochl, O. Jepsen, O.K. Anderson, *Phys. Rev. B* **49**, 16223 (1994).

[22] F.D. Murnaghan, *Proc. Natl. Acad. Sci. USA* **30**, 244 (1944).

[23] AH. Reshak, M. Jamal, *J. Alloys Comp.* **543**, 147 (2012).

[24] G. Grimvall, *Thermophysical Properties of Materials*, Elsevier, Amsterdam 1999, enlarged and revised edition.

[25] A. Meziani, H. Belkhir, *Comput. Mater. Sci.* **61**, 67 (2012).

[26] B. Ghebouli, M.A. Ghebouli, M. Fatmi, A. Bouhemadou, *Solid State Commun.* **150**, 1896 (2010).

[27] M.A. Ghebouli, B. Ghebouli, M. Fatmi, *Physica B* **406**, 1837 (2011).

[28] B. Mayer, H. Anton, E. Bott, M. Methfessel, J. Sticht, P.C. Schmidt, *Intermetallics* **11**, 23 (2003).

[29] J. Haines, J.M. Leger, G. Bocquillon, *Annu. Rev. Mater. Res.* **31**, 1 (2001).

[30] S.F. Pugh, *Philos. Mag.* **45**, 823 (1954).

[31] M.A. Macdonald, E.N. Melchakov, I.H. Munro, P.A. Rodnyi, A.S. Voloshinovsky, *J. Lumin.* **65**, 19 (1995).

[32] K. Ephraim Babu, A. Veeraiah, D. Tirupati Swamy, V. Veeraiah, *Chin. Phys. Lett.* **29**, 117102 (2012).

[33] K. Ephraim Babu, A. Veeraiah, D. Tirpathi Swamy, V. Veeraiah, *Mater. Sci.-Poland* **30**, 359 (2012).

[34] N.V. Smith, *Phys. Rev. B* **3**, 1862 (1971).

[35] C. Ambrosch-Draxl, J.O. Sofo, *Comput. Phys. Commun.* **175**, 1 (2006).

[36] M. Fox, *Optical Properties of Solids*, Oxford University Press, New York 2001.

[37] F. Wooten, *Optical Properties of Solids*, Academic Press, New York 1972.

[38] M. Maqbool, B. Amin, I. Ahmad, *J. Opt. Soc. Am. B* **26**, 2180 (2009).

[39] M. Maqbool, M.E. Kordesch, A. Kayani, *J. Opt. Soc. Am. B* **26**, 998 (2009).

[40] G. Shwetha, V. Kanchana, *Phys. Rev. B* **86**, 115209 (2012).